

Molecular structures of supported niobium oxide catalysts under ambient conditions

Jih-Mirn Jehng and Israel E. Wachs*

Zettlemoyer Center for Surface Studies, Department of Chemical Engineering, Lehigh University, Bethlehem, PA 18015 (U.S.A.)

(Received October 10, 1990; revised November 28, 1990)

Abstract

The supported niobium oxide catalysts were investigated by Raman spectroscopy and X-ray photoelectron spectroscopy in order to determine the molecular structure and monolayer coverage of the surface niobium oxide phase on oxide supports (MgO, Al₂O₃, TiO₂, ZrO₂, and SiO₂). The molecular structures of the surface niobium oxide phases present in the supported niobium oxide catalysts under ambient conditions, where adsorbed moisture is present, are controlled by the surface pH of the system. Basic surfaces result in the formation of highly distorted NbO₆ groups and acidic surfaces result in the formation of slightly distorted NbO₆, NbO₇ and NbO₈ groups. The surface niobium oxide overlayer is stable to high calcination temperatures due to the strong surface niobium oxide–support interaction. The monolayer coverage of supported niobium oxide catalysts is reached at ~19 wt.% Nb₂O₅/Al₂O₃, ~7 wt.% Nb₂O₅/TiO₂, ~5 wt.% Nb₂O₅/ZrO₂ and ~2 wt.% Nb₂O₅/SiO₂, but not for the Nb₂O₅/MgO system due to the incorporation of Nb⁺⁵ into the MgO support.

Introduction

Supported niobium oxide catalysts possess a surface niobium oxide overlayer on a high surface area oxide support. The surface niobium oxide phase is formed by the reaction of a suitable niobium precursor (*e.g.* oxalate [1], alkoxide [2] or chloride [3]) with the surface hydroxyls of the oxide support [4]. The physical and chemical properties of the surface niobium oxide can be quite different than those found in bulk Nb₂O₅ phases, and can also dramatically influence the properties of the oxide supports [5]. For example, the surface niobium oxide phases impart thermal stability to oxide supports (*e.g.*, Al₂O₃ and TiO₂) at elevated temperatures [6, 7], form strong acid centers on oxide supports [6, 8–10], and are active for numerous catalytic reactions in the petrochemical (*e.g.* olefin metathesis, dimerization, trimerization, isomerization, as well as hydration and dehydration), petroleum (*e.g.* cracking, isomerization and alkylation), and pollution control (NO_x reduction from stationary emissions) industries [5].

The molecular structures of the surface niobium oxide phases, however, have not received much attention and only preliminary Raman [1, 7] and

*Author to whom correspondence should be addressed.

EXAFS [11, 12] characterization studies have been reported. The multiple surface niobium oxide phases that simultaneously coexist in the supported niobium oxide catalysts have generated confusion in the understanding of supported niobium oxide materials. This confusion results from the lack of systematic studies on niobium oxide reference compounds and supported niobium oxide materials.

The niobium oxide structure–Raman spectra relationships and niobium oxide solution chemistry have been previously reported [13, 14]. In the present study, the molecular structures of the surface niobium oxide phases on Al_2O_3 , TiO_2 , ZrO_2 , MgO and SiO_2 supports will be investigated under ambient conditions with Raman spectroscopy as a function of Nb_2O_5 loading and calcination temperature. The supported metal oxide catalysts contain adsorbed moisture under ambient conditions which influence the molecular structures of the surface metal oxide phases [13, 15]. These structures are directly related to the various aqueous metal oxide species [16]. Thus, the molecular structures of the surface niobium oxide phases under ambient conditions can be determined by the comparison of Raman spectra between the surface niobium oxide phases and the various niobium oxide species present in aqueous solutions at different solution pH.

The supported niobium oxide catalysts will be further investigated by the BET surface area measurement and X-ray photoelectron spectroscopy (XPS) in order to determine the monolayer content of these catalysts. The formation of the surface niobium oxide overlayer can stabilize the high surface areas of the oxide supports at elevated calcination temperatures. XPS is a surface-sensitive technique, and provides the information on composition, oxidation state and dispersion of the surface niobium oxide phases [17, 18]. Raman studies also indicate that a monolayer of surface niobium oxide phases is reached due to the detection of crystalline Nb_2O_5 .

Experimental

Materials and methods

Niobium oxalate was supplied by Niobium Products Co. (Pittsburgh, PA) with the following chemical analysis: 20.5% Nb_2O_5 , 790 ppm Fe, 680 ppm Si and 0.1% insolubles. Niobium ethoxide (99.999% purity) was purchased from Johnson Matthey (Ward Hill, MA). The oxide supports employed in the present investigation are: MgO (Fluka, $\sim 80 \text{ m}^2 \text{ g}^{-1}$ after calcination at $700 \text{ }^\circ\text{C}$ for 2 h), Al_2O_3 (Harshaw, $\sim 180 \text{ m}^2 \text{ g}^{-1}$ after calcination at $500 \text{ }^\circ\text{C}$ for 16 h), TiO_2 (Degussa, $\sim 50 \text{ m}^2 \text{ g}^{-1}$ after calcination at $450 \text{ }^\circ\text{C}$ for 2 h), ZrO_2 (Degussa, $\sim 39 \text{ m}^2 \text{ g}^{-1}$ after calcination at $450 \text{ }^\circ\text{C}$ for 2 h), and SiO_2 (Cab-O-Sil, $\sim 275 \text{ m}^2 \text{ g}^{-1}$ after calcination at $500 \text{ }^\circ\text{C}$ for 16 h).

The TiO_2 , ZrO_2 , Al_2O_3 and SiO_2 -supported niobium oxide catalysts were prepared by the incipient-wetness impregnation method using niobium oxalate/oxalic acid aqueous solutions (aqueous preparation) [1]. The water-sensitive MgO support required the use of nonaqueous niobium ethoxide/propanol

solutions under a nitrogen environment for the preparation of the Nb₂O₅/MgO catalysts. The supported niobium oxide on Al₂O₃ catalysts were also prepared by the nonaqueous niobium ethoxide/propanol solution in order to compare the aqueous and nonaqueous preparation methods.

For the aqueous preparation method the samples were initially dried at room temperature for 16 h, further dried at 110–120 °C for 16 h, and calcined at 450 °C (Nb₂O₅/TiO₂ and Nb₂O₅/ZrO₂, 2 h) or at 500 °C (Nb₂O₅/Al₂O₃ and Nb₂O₅/SiO₂, 16 h) under flowing dry air. For the nonaqueous preparation method, the samples were initially dried at room temperature for 16 h, further dried at 110–120 °C for 16 h under flowing N₂, then calcined at 500 °C for 1 h under flowing N₂ and for 15 h (Nb₂O₅/Al₂O₃) or for 1 h (Nb₂O₅/MgO) under flowing dry air.

BET surface area measurement

The BET surface areas of the supported niobium oxide catalysts were obtained with a Quantsorb surface area analyzer (Quantachrome corporation, Model OS-9) using a 3:7 ratio of N₂/He mixture as a probe gas. Typically, 0.200–0.300 g of sample was used for the measurement and the sample was outgassed at 250 °C prior to N₂ adsorption.

Raman spectroscopy

Raman spectra were obtained with a Spex Triplemate spectrometer (Model 1877) coupled to an EG&G intensified photodiode array detector, cooled thermoelectrically to –35 °C, and interfaced with an EG&G OMA III Optical Multichannel Analyzer (Model 1463). The samples were excited by the 514.5 nm line of the Ar⁺ laser with 10–100 mW of power. The laser beam was focused on the sample illuminator, in which the sample typically spins at about 2000 rpm to avoid local heating, and was reflected into the spectrometer by a 90° angle with the incident light. The scattered Raman light was collected by the spectrometer at room temperature, and analyzed with an OMA III software package. The overall spectral resolution of the spectra was determined to be about 2 cm⁻¹. Additional details about the Raman spectrometer can be found elsewhere [19].

X-ray photoelectron spectroscopy (XPS)

XPS experiments on the Al₂O₃-supported niobium oxide catalysts were performed on a Physical Electronic Instruments ESCA/Auger system. The samples were placed on the sample holder at a 45° angle to the entrance of the analyzer and the system was evacuated to 10⁻⁹–10⁻¹⁰ torr. The XPS spectra were calibrated against the Au 4f_{7/2} photoelectron line using the Mg K α exciting radiation from a dual anode operating at 10 kV, 40 mA. XPS experiments on the MgO, TiO₂, ZrO₂ and SiO₂-supported niobium oxide catalysts were performed on a VG ESCALAB I instrument with Al K α exciting radiation from a dual anode operating at 14 kV, 40 mA. The samples were placed on the sample holder at a 90° angle to the entrance of the analyzer and the system was evacuated to 10⁻⁹–10⁻¹⁰ torr. The XPS spectra were calibrated against the C_{1s} photoelectron line.

Peak areas were determined from the background-subtracted spectra and corrected using instrument-dependent sensitivity factors. The $(\text{Nb}/\text{M})_{\text{surface}}$, where M is Mg, Al, Ti, Zr or Si, ratios of the supported niobium oxide catalysts were obtained by integrating the areas of the most intense photoelectron lines of Nb $3d_{3/2, 5/2}$ and M (Mg 2s, Al 2p, Ti $2p_{3/2}$, Zr 3d and Si 2p), and the $(\text{Nb}/\text{M})_{\text{bulk}}$ ratios were calculated from the total concentration of Nb^{+5} atom which was impregnated onto the oxide supports.

Results

BET surface area measurements

The BET surface areas of the supported niobium oxide catalysts are shown in Fig. 1 as a function of Nb_2O_5 loading. The results reveal that the high surface areas of the oxide supports (such as MgO, Al_2O_3 , TiO_2 , ZrO_2 and SiO_2) are maintained after the addition of niobium oxide. For the $\text{Nb}_2\text{O}_5/\text{Al}_2\text{O}_3$ system, the aqueously prepared samples possess a slightly lower surface area at high niobium oxide loadings than the nonaqueously prepared samples.

The presence of the surface niobium oxide overlayer retards the loss in surface areas of the Al_2O_3 , TiO_2 , ZrO_2 and SiO_2 supports at elevated calcination temperatures, but not for the MgO support, as shown in Table 1. The addition of niobium oxide on the MgO support results in a dramatic decrease in surface area at high calcination temperatures.

X-ray photoelectron spectroscopy

The $(\text{Nb}/\text{M})_{\text{surface}}$ vs. $(\text{Nb}/\text{M})_{\text{bulk}}$, where M is Mg, Al, Ti, Zr or Si, curves of the supported niobium oxide catalysts are shown in Fig. 2. For the $\text{Nb}_2\text{O}_5/\text{MgO}$ system, the $(\text{Nb}/\text{Mg})_{\text{surface}}$ ratio linearly increases over the entire range

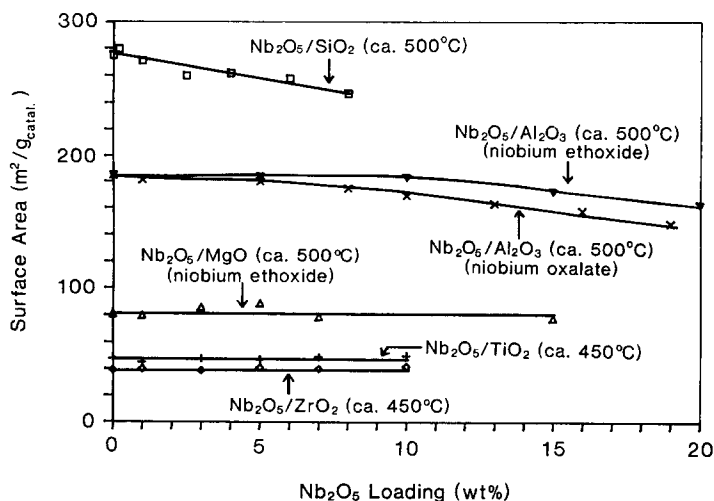


Fig. 1. Surface areas of the supported niobium oxide catalysts as a function of Nb_2O_5 loading.

TABLE 1

The influence of calcination temperature on the surface areas ($\text{m}^2 \text{g}^{-1}$) of supported niobium oxide catalysts

Catalyst	Calcination temperature ($^{\circ}\text{C}$)			
	450	500	700	950
MgO	—	241	81	49
5 wt.% $\text{Nb}_2\text{O}_5/\text{MgO}^{\text{a}}$	—	89	80	16
Al_2O_3	—	185	—	98
5 wt.% $\text{Nb}_2\text{O}_5/\text{Al}_2\text{O}_3^{\text{b}}$	—	180	—	105
TiO_2	50	—	24	6
5 wt.% $\text{Nb}_2\text{O}_5/\text{TiO}_2^{\text{a}}$	47	—	38	10
ZrO_2	39	—	22	9
3 wt.% $\text{Nb}_2\text{O}_5/\text{ZrO}_2^{\text{a}}$	39	—	34	19
SiO_2	—	275	—	127
1 wt.% $\text{Nb}_2\text{O}_5/\text{SiO}_2^{\text{b}}$	—	271	—	181

^aCalcined for 2 h.

^bCalcined for 16 h.

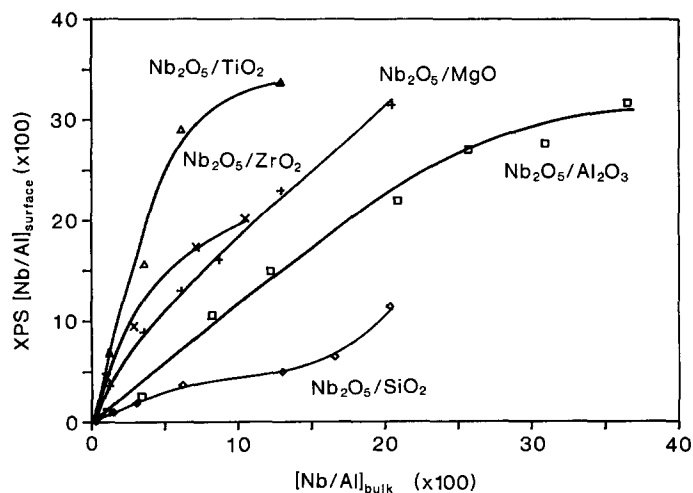


Fig. 2. X-ray photoelectron spectroscopy analysis of supported niobium oxide catalysts.

of Nb_2O_5 loading. For the $\text{Nb}_2\text{O}_5/\text{Al}_2\text{O}_3$ system, the $(\text{Nb}/\text{Al})_{\text{surface}}$ ratio linearly increases with increasing Nb_2O_5 loading to ~ 19 wt.%, and deviates from the linear curve at high loadings due to the formation of bulk Nb_2O_5 particles. Similarly, the $\text{Nb}_2\text{O}_5/\text{TiO}_2$, $\text{Nb}_2\text{O}_5/\text{ZrO}_2$ and $\text{Nb}_2\text{O}_5/\text{SiO}_2$ systems deviate from linearity at ~ 7 wt.%, ~ 5 wt.% and ~ 2 wt.% Nb_2O_5 , respectively.

Raman spectroscopy

Nb_2O_5/MgO

The Raman spectra of magnesium oxide-supported niobium oxide are shown in Fig. 3 as a function of Nb_2O_5 loading. The Raman bands at ~ 875 , ~ 450 , ~ 380 and ~ 230 cm^{-1} are associated with the surface niobium oxide phases, since MgO is not Raman active, and increase with Nb_2O_5 loading. The Raman bands at ~ 1085 and ~ 280 cm^{-1} are due to $CaCO_3$ and decrease with Nb_2O_5 loading. The Raman spectra of 5 wt.% Nb_2O_5/MgO calcined at different temperatures are shown in Fig. 4. The surface niobium oxide phase

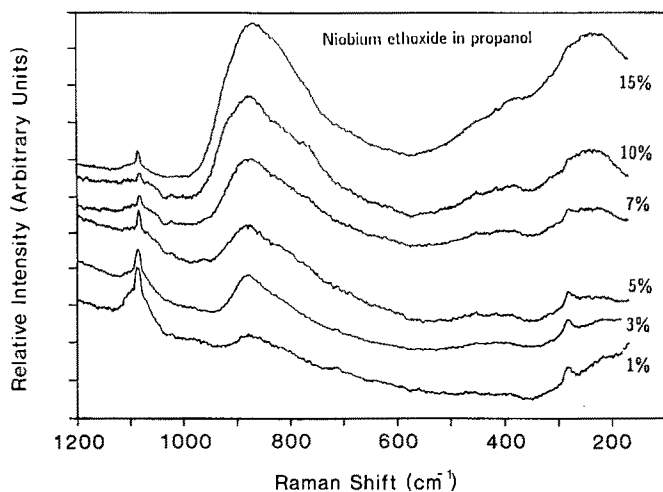


Fig. 3. Raman spectra of MgO-supported niobium oxide (calcined at 500 °C) as a function of Nb_2O_5 loading.

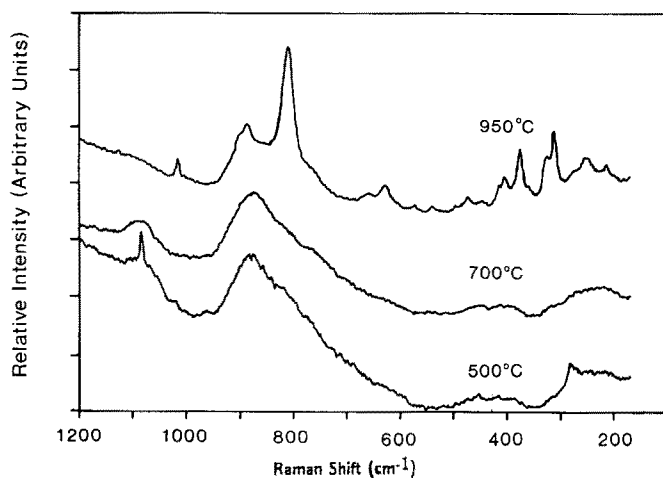


Fig. 4. Raman spectra of 5 wt.% Nb_2O_5/MgO as a function of calcination temperature.

Raman bands (~ 875 , ~ 450 , ~ 380 and ~ 230 cm^{-1}) remain at the same positions after treatments at 500 and 700 $^{\circ}\text{C}$, while the CaCO_3 Raman bands (~ 1085 and ~ 280 cm^{-1}) disappear after the 700 $^{\circ}\text{C}$ calcination. For the 950 $^{\circ}\text{C}$ calcined sample, multiple strong and sharp Raman bands appear in the 200–1000 cm^{-1} region (suggesting the formation of a Mg–Nb–O solid solution).

$\text{Nb}_2\text{O}_5/\text{Al}_2\text{O}_3$

The Raman spectra of the aqueously prepared alumina-supported niobium oxide are shown in Fig. 5. For Nb_2O_5 loadings less than 5 wt.%, broad and weak Raman bands due to the surface niobium oxide phase (since the Al_2O_3 support is not Raman active) appear at ~ 900 and ~ 230 cm^{-1} , and between 5 and 8 wt.% $\text{Nb}_2\text{O}_5/\text{Al}_2\text{O}_3$ the Raman band at ~ 900 cm^{-1} shifts to ~ 930 cm^{-1} . For Nb_2O_5 loadings greater than 8 wt.%, the Raman band at ~ 930 cm^{-1} shifts to ~ 890 cm^{-1} , an additional Raman band from the surface niobium oxide phase appears at ~ 645 cm^{-1} and increases in intensity with Nb_2O_5 loading. The intensity of the Raman band at ~ 230 cm^{-1} also increases with Nb_2O_5 loading. The Raman spectra of the nonaqueously prepared alumina-supported niobium oxide catalysts are shown in Fig. 6, and reveal that the nonaqueously prepared catalysts possess the same Raman features as the aqueously prepared samples.

The influence of the calcination temperature upon the 5 wt.% $\text{Nb}_2\text{O}_5/\text{Al}_2\text{O}_3$ sample is shown in Fig. 7. The surface niobium oxide phase Raman bands at ~ 900 and ~ 230 cm^{-1} are stable to elevated calcination temperature. However, the Raman band at ~ 900 cm^{-1} shifts to ~ 930 cm^{-1} in the 950 $^{\circ}\text{C}$ -calcined sample and additional Raman bands appear at ~ 850 , ~ 750 , ~ 645 and ~ 250 cm^{-1} due to the formation of $\theta, \delta\text{-Al}_2\text{O}_3$ [20].

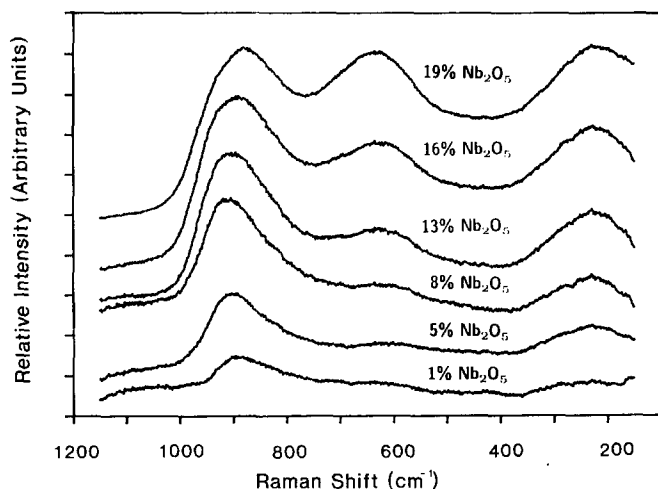


Fig. 5. Raman spectra of aqueously prepared Al_2O_3 -supported niobium oxide (calcined at 500 $^{\circ}\text{C}$) as a function of Nb_2O_5 loading.

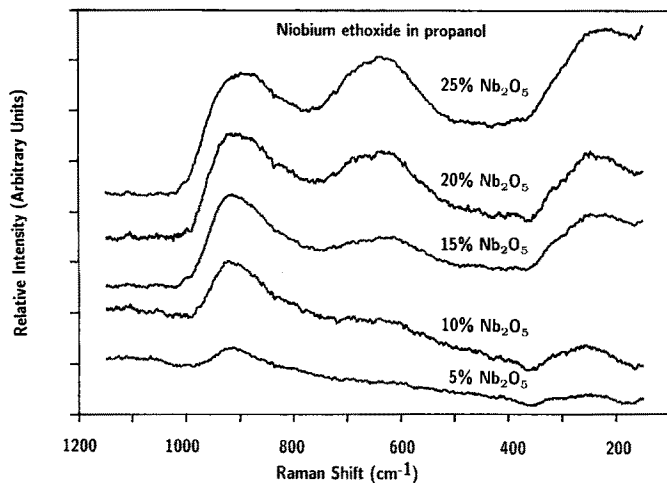


Fig. 6. Raman spectra of nonaqueously prepared Al₂O₃-supported niobium oxide (calcined at 500 °C) as a function of Nb₂O₅ loading.

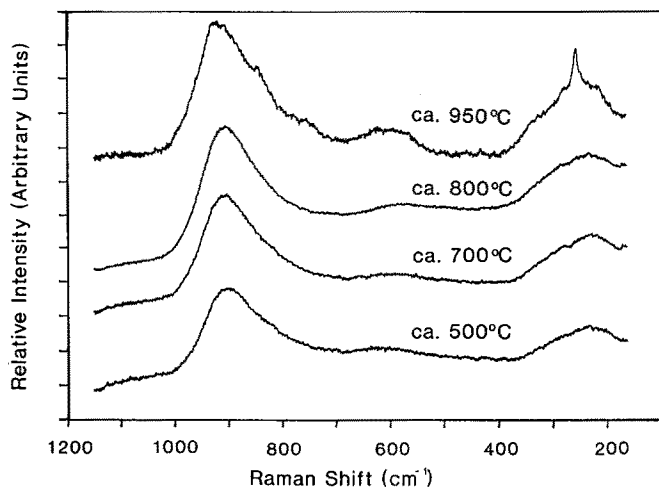


Fig. 7. Raman spectra of 5 wt.% Nb₂O₅/Al₂O₃ as a function of calcination temperature.

Nb₂O₅/TiO₂

The Raman data for titania-supported niobium oxide catalysts was collected only in the 700–1200 cm⁻¹ region because of the strong scattering from the TiO₂ support below 700 cm⁻¹. The Raman spectra of titania-supported niobium oxide are shown in Fig. 8 as a function of Nb₂O₅ loading. The weak titania (anatase or rutile) Raman features in the 700–1200 cm⁻¹ region were subtracted from the spectrum in order to more clearly observe the Raman features of the surface niobium oxide phase. A weak and broad Raman band appears at ~895 cm⁻¹ from the surface niobium oxide phase which shifts from ~895 to ~930 cm⁻¹ upon increasing the Nb₂O₅ loading

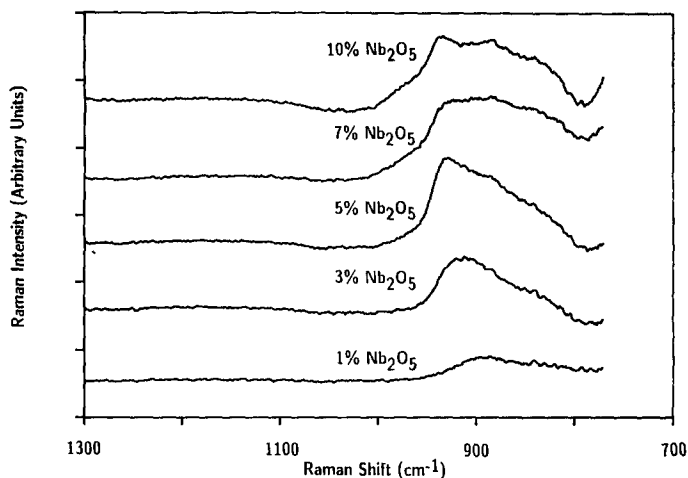


Fig. 8. Raman spectra of TiO₂-supported niobium oxide (calcined at 450 °C) as a function of Nb₂O₅ loading.

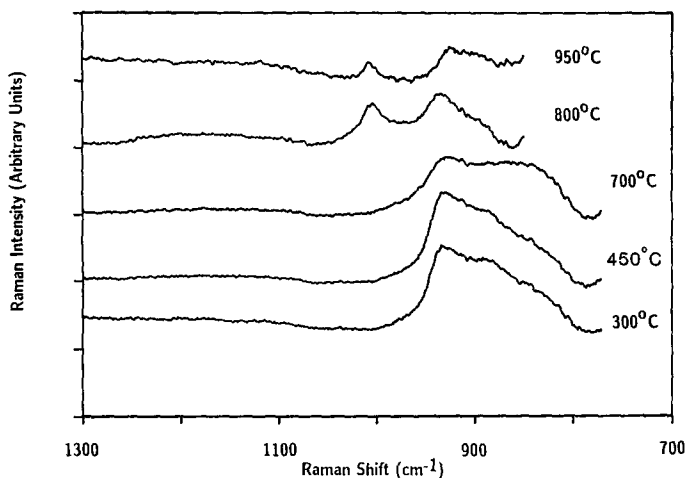


Fig. 9. Raman spectra of 5 wt.% Nb₂O₅/TiO₂ as a function of calcination temperature.

to 5 wt.%. For Nb₂O₅ loadings greater than 5 wt.%, an additional weak and broad Raman band appears at ~ 870 cm⁻¹ from the surface niobium oxide phase.

The Raman spectra of 5 wt.% Nb₂O₅/TiO₂ after different calcination temperatures are shown in Fig. 9. The surface niobium oxide phase Raman band at ~ 930 cm⁻¹ retains the same position after calcination between 300 to 700 °C, but an additional weak and broad Raman band at ~ 870 cm⁻¹ appears after the 700 °C calcination. For temperature treatments greater than 700 °C, an additional weak and sharp Raman band appears at ~ 1000 cm⁻¹ and its intensity decreases slightly with further calcination at 950 °C.

The Raman features of bulk TiO_2 , in the $700\text{--}100\text{ cm}^{-1}$ region, are also changed after $800\text{ }^\circ\text{C}$ calcination indicating that the phase transformation from anatase (~ 639 , ~ 517 , ~ 398 , and $\sim 144\text{ cm}^{-1}$) to rutile (~ 614 , ~ 445 , and $\sim 240\text{ cm}^{-1}$) of TiO_2 is detected at $800\text{ }^\circ\text{C}$ calcination.

$\text{Nb}_2\text{O}_5/\text{ZrO}_2$

The Raman spectra of zirconia-supported niobium oxide catalysts was also collected only in the $750\text{--}1200\text{ cm}^{-1}$ region because of the strong scattering of ZrO_2 . The ZrO_2 support possesses a weak Raman band at $\sim 755\text{ cm}^{-1}$ which arises from the first overtone of its strong Raman band at $\sim 380\text{ cm}^{-1}$. The Raman spectra were not corrected for the ZrO_2 background because of the overlapping Raman band between the ZrO_2 support and the surface niobium oxide phase. The Raman spectra of zirconia-supported niobium oxide catalysts are shown in Fig. 10 as a function of Nb_2O_5 loading. The surface niobium oxide phase possesses a weak and broad Raman band at $\sim 875\text{ cm}^{-1}$ which shifts from ~ 875 to $\sim 920\text{ cm}^{-1}$ with increasing Nb_2O_5 loadings.

The influence of the calcination temperatures upon the 3 wt.% $\text{Nb}_2\text{O}_5/\text{ZrO}_2$ sample is shown in Fig. 11. The surface niobium oxide phase Raman band appearing at 900 cm^{-1} shifts to $\sim 930\text{ cm}^{-1}$ upon increasing the calcination temperature from 450 to $950\text{ }^\circ\text{C}$ and an additional broad Raman band at $\sim 820\text{ cm}^{-1}$ appears after the $950\text{ }^\circ\text{C}$ calcination.

$\text{Nb}_2\text{O}_5/\text{SiO}_2$

The Raman spectra of silica-supported niobium oxide catalysts after calcination at $500\text{ }^\circ\text{C}$ are shown in Fig. 12. For Nb_2O_5 loadings less than 2 wt.%, a weak and broad Raman band appears at $\sim 960\text{ cm}^{-1}$, and at higher loading additional Raman bands appear at ~ 650 and $\sim 240\text{ cm}^{-1}$. Upon

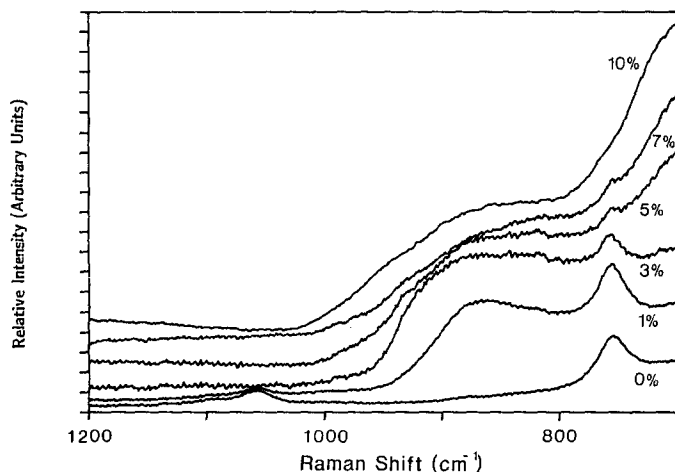


Fig. 10. Raman spectra of ZrO_2 -supported niobium oxide (calcined at $450\text{ }^\circ\text{C}$) as a function of Nb_2O_5 loading.

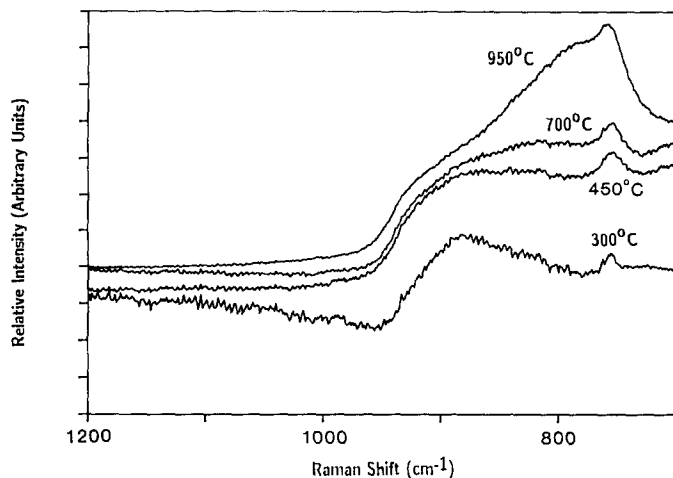


Fig. 11. Raman spectra of 3 wt.% Nb₂O₅/ZrO₂ as a function of calcination temperature.

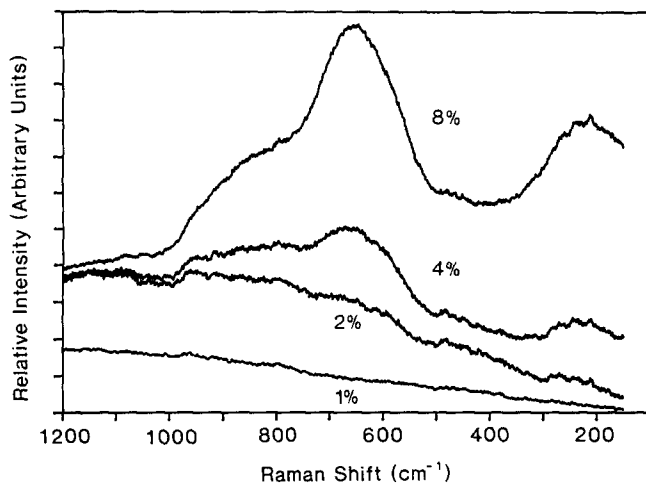


Fig. 12. Raman spectra of SiO₂-supported niobium oxide (calcined at 500 °C) as a function of Nb₂O₅ loading.

increasing the Nb₂O₅ loading to 8 wt.%, the surface niobium oxide phase has Raman features (~ 900 , ~ 650 and ~ 240 cm⁻¹) similar to bulk Nb₂O₅ (amorphous) [13]. The silica-supported niobium oxide catalysts were further calcined at 600 °C in order to observe better Raman scattering of the surface niobium oxide phase, as shown in Fig. 13. At low Nb₂O₅ loading (< 2 wt.%), the Raman intensity at ~ 960 cm⁻¹ increases with increasing Nb₂O₅ loading and remains constant with further increases in Nb₂O₅ loading. At high Nb₂O₅ loading (> 2 wt.%), the Raman band at ~ 900 cm⁻¹ disappears and the Raman band at ~ 650 cm⁻¹ shifts to ~ 680 cm⁻¹, indicating the phase transformation of amorphous Nb₂O₅ to TT-Nb₂O₅ [13].

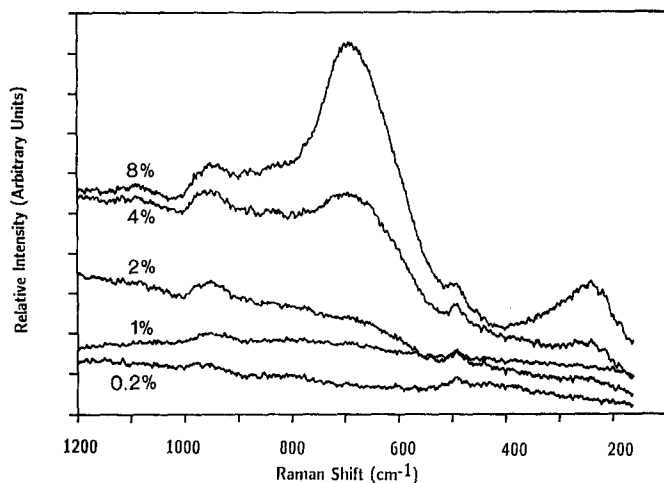


Fig. 13. Raman spectra of SiO₂-supported niobium oxide (calcined at 600 °C) as a function of Nb₂O₅ loading.

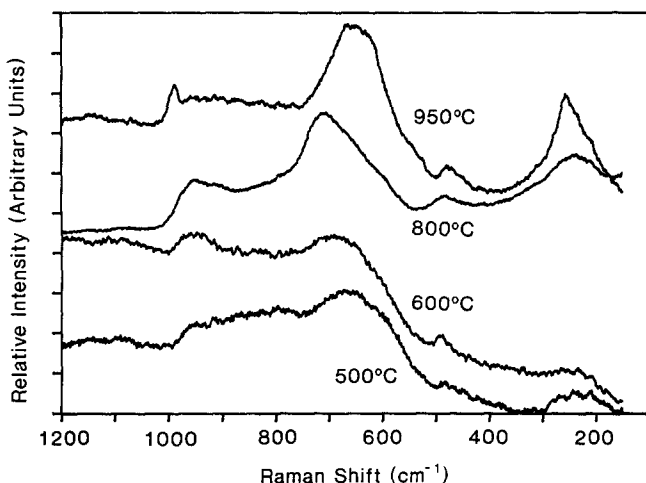


Fig. 14. Raman spectra of 4 wt.% Nb₂O₅/SiO₂ as a function of calcination temperature.

The Raman spectra of the 4 wt.% Nb₂O₅/SiO₂ sample are shown in Fig. 14 as a function of calcination temperature. The Raman band at ~ 960 cm⁻¹ retains the same positions, but becomes stronger with increasing temperature treatment. Upon increasing the calcination temperature to 950 °C, bulk Nb₂O₅ on silica support has a phase transformation order similar to Nb₂O₅·*n*H₂O [13]: amorphous Nb₂O₅ (~ 900 , ~ 650 and ~ 240 cm⁻¹), TT-Nb₂O₅ (~ 680 and ~ 240 cm⁻¹), T-Nb₂O₅ (~ 700 and ~ 240 cm⁻¹) and H-Nb₂O₅ (~ 993 , ~ 670 , ~ 625 and ~ 260 cm⁻¹).

Discussion

The nature of the surface niobium oxide phase is determined from a comparison of the Raman spectra of the MgO, Al₂O₃, TiO₂, ZrO₂ and SiO₂-supported niobium oxide samples with those of niobium oxide reference compounds and solution chemistry [13, 14]. The 1–15% Nb₂O₅/MgO, 1–19% Nb₂O₅/Al₂O₃, 1–5% Nb₂O₅/ZrO₂ and 0.2–2% Nb₂O₅/SiO₂ samples after calcination at 450 or 500 °C do not contain the Raman features of crystalline Nb₂O₅ phases (major band at ~690 cm⁻¹ due to slightly distorted NbO₆ octahedra), but possess weak and broad Raman bands in the 900–1000 cm⁻¹ region characteristic of a two-dimensional surface niobium oxide phase. The 1–10% Nb₂O₅/TiO₂ samples also possess weak and broad Raman bands in the 890–930 cm⁻¹ region which are characteristic of a two-dimensional surface niobium oxide phase. However, the very strong TiO₂ Raman scattering below 700 cm⁻¹ prevented the identification of crystalline Nb₂O₅ phases.

XPS studies reveal that a linear relation between the (Nb/Al)_{surface} ratios and (Nb/Al)_{bulk} ratios (see Fig. 2) are observed due to the formation of a two-dimensional niobium oxide overlayer [17, 18]. The break in the linear curve corresponding to ~19 wt.% Nb₂O₅ loading suggests that the transition from a two-dimensional overlayer to three-dimensional particles (monolayer coverage) occurs at this point [17, 18]. This conclusion is supported by XRD measurements, which detect only crystalline Nb₂O₅ particles above ~19 wt.% Nb₂O₅/Al₂O₃, and CO₂ chemisorption measurements [1], which indicate that the basic alumina hydroxyls have been removed by the niobium oxide overlayer at ~19 wt.% Nb₂O₅/Al₂O₃ [21, 22]. The XPS surface measurements of the Nb₂O₅/TiO₂, Nb₂O₅/ZrO₂ and Nb₂O₅/SiO₂ systems (see Fig. 2) also suggest that the monolayer coverage of these three systems approaches ~7, ~5 and ~2 wt.% Nb₂O₅ loading, respectively. The increase in the [Nb/Si]_{surface} ratio at 12 wt.% Nb₂O₅/SiO₂ is due to the aggregation of bulk Nb₂O₅ on the exterior of the silica particles. However, no break is observed in the curve of [Nb/Mg]_{surface} *vs.* [Nb/Mg]_{bulk}, and the linear increase in [Nb/Mg]_{surface} with increasing Nb₂O₅ loading indicates that Nb⁺⁵ is incorporated into the MgO support surface.

Under ambient conditions, surface metal oxide overlayers on oxide supports are hydrated due to the presence of adsorbed moisture, and the moisture influences the molecular structures of these metal oxide phases [13, 15]. The Raman frequencies of the supported niobium oxide catalysts under ambient conditions, after calcination at 450 or 500 °C, are tabulated in Table 2. Recent Raman characterization studies of supported vanadium oxide, molybdenum oxide, tungsten oxide and chromium oxide catalysts under ambient conditions have demonstrated that the molecular structures of the hydrated surface metal oxide phases are directly related to the surface pH of the aqueous film, which is determined by the combined pH of the oxide support and the metal oxide overlayer [16].

In aqueous environments, the oxide support equilibrates at the pH which results in net zero surface charge (point zero surface charge or isoelectric

TABLE 2

Raman bands of supported niobium oxide catalysts under ambient conditions

Catalyst	BET surface area ($\text{m}^2/\text{g}_{\text{catal.}}$)	Raman bands (cm^{-1})
5% $\text{Nb}_2\text{O}_5/\text{MgO}$	86	880(m), 450(w), 380(w), 230(w)
10% $\text{Nb}_2\text{O}_5/\text{MgO}$	75	880(s), 450(w), 380(w), 230(m)
5% $\text{Nb}_2\text{O}_5/\text{Al}_2\text{O}_3$	180	900(s), 230(m)
19% $\text{Nb}_2\text{O}_5/\text{Al}_2\text{O}_3$	151	890(s), 650(s), 230(s)
1% $\text{Nb}_2\text{O}_5/\text{TiO}_2$	48	895(w)
7% $\text{Nb}_2\text{O}_5/\text{TiO}_2$	45	930(w)
1% $\text{Nb}_2\text{O}_5/\text{ZrO}_2$	39	875(w)
5% $\text{Nb}_2\text{O}_5/\text{ZrO}_2$	40	920(w)
2% $\text{Nb}_2\text{O}_5/\text{SiO}_2$	265	960(w)
4% $\text{Nb}_2\text{O}_5/\text{SiO}_2$	262	960(w), 680(m), 230(w)

point). The pH at the point zero surface charge of the metal oxide supports and niobium oxide are [23, 24]:

Support	pH of point zero surface charge
MgO	12
Al_2O_3	9
TiO_2	6.0–6.4
ZrO_2	4–7
SiO_2	~ 2
Nb_2O_5	~ 0.5

For supported metal oxide catalyst, the point zero surface charge of such composite materials is determined by the combined pH of the oxide support and the metal oxide overlayer. The influence of the metal oxide overlayer on the point zero surface charge of the composite system is directly related to the surface coverage of the surface metal oxide phases [25]. Thus, the addition of surface niobium oxide ($\text{pH} \sim 0.5$) to oxide supports ($2 < \text{pH} < 12$) will always decrease the pH of the point zero surface charge, and the decrease will be proportional to the surface niobium oxide coverage.

At low surface niobium oxide coverages of the supported niobium oxide catalysts, the surface pH under ambient conditions is dominated by the properties of the oxide support. The basic pH values of the MgO ($\text{pH} = 12$) and Al_2O_3 ($\text{pH} = 9$) supports suggest that hexaniobate species ($\text{H}_x\text{Nb}_6\text{O}_{19}^{-(8-x)}$ where $x = 1, 2, 3$) should be present with corresponding Raman bands at $\sim 880 \text{ cm}^{-1}$ [14, 26, 27]. Indeed, at low surface coverages for $\text{Nb}_2\text{O}_5/\text{MgO}$ and $\text{Nb}_2\text{O}_5/\text{Al}_2\text{O}_3$, only strong Raman bands are present at ~ 880 and ~ 900

cm^{-1} respectively (see Table 2). The somewhat acidic pH values of the TiO_2 (pH=6.0–6.4) and ZrO_2 (pH=4–7) supports suggest that the hexaniobate species should not be present in high concentrations [14, 26, 27] and that $\text{Nb}_2\text{O}_5 \cdot n\text{H}_2\text{O}$ -type structures, containing slightly distorted NbO_6 as well as NbO_7 and NbO_8 groups, should be present at $\sim 650 \text{ cm}^{-1}$ for $\text{Nb}_2\text{O}_5/\text{TiO}_2$ and $\text{Nb}_2\text{O}_5/\text{ZrO}_2$ at low surface coverages. Unfortunately, the strong vibrations of the TiO_2 and ZrO_2 supports in this region do not allow direct confirmation of such niobium oxide species. However, the rather weak Raman bands for $\text{Nb}_2\text{O}_5/\text{TiO}_2$ and $\text{Nb}_2\text{O}_5/\text{ZrO}_2$ at ~ 895 and $\sim 875 \text{ cm}^{-1}$, respectively, are consistent with this conclusion. For the acidic SiO_2 support with a pH value of ~ 3.9 , $\text{Nb}_2\text{O}_5 \cdot n\text{H}_2\text{O}$ -type structures with Raman band at $\sim 650 \text{ cm}^{-1}$ would be expected, but a weak and broad Raman band appearing at $\sim 960 \text{ cm}^{-1}$ instead of $\sim 650 \text{ cm}^{-1}$ is observed (see Figs. 12 and 13). This indicates that the surface niobium oxide phase on silica, after treatment with 500 or 600 °C calcination, contains a highly distorted NbO_6 octahedra which is similar to the 'capping' structure of layered niobium oxide reference compound [13]. The transformation of the structure of the surface niobium oxide phase, from a slightly distorted NbO_6 octahedra to a highly distorted NbO_6 octahedra, on SiO_2 under high-temperature treatments is probably due to the weak interaction between the surface niobium oxide phase and the SiO_2 support, and the presence of the surface niobium oxide phase, possessing a highly distorted NbO_6 octahedra, on SiO_2 under ambient conditions is probably due to the hydrophobicity of SiO_2 .

Gil-Llambias *et al.* have shown that the surface pH of the Al_2O_3 -supported V_2O_5 and MoO_3 and the TiO_2 -supported V_2O_5 and MoO_3 systems decreases with increasing surface vanadium oxide coverage [25]. The surface pH of the supported vanadium oxide system is expected to be lower than the surface pH of the oxide support at high surface coverages, because the surface pH of $\text{V}_2\text{O}_5 \sim 1.5$, and close to the oxide support at low surface coverages. Consequently, the surface pH of the supported niobium oxide catalysts under ambient conditions is significantly influenced by the acidic niobium oxide overlayer at high surface niobium oxide coverages. Under acidic aqueous conditions the $\text{Nb}_2\text{O}_5 \cdot n\text{H}_2\text{O}$ -type structures, containing slightly distorted NbO_6 as well as NbO_7 and NbO_8 groups, should be present and give rise to a Raman band at $\sim 650 \text{ cm}^{-1}$ [13]. Indeed, such Raman bands are observed at high loading for $\text{Nb}_2\text{O}_5/\text{Al}_2\text{O}_3$ and $\text{Nb}_2\text{O}_5/\text{SiO}_2$ catalysts. The thermal stabilities of these niobium oxide structures, however, are very different on the SiO_2 and Al_2O_3 structures. For $\text{Nb}_2\text{O}_5/\text{SiO}_2$, further calcination at 700 °C shifts the Raman band from ~ 680 to $\sim 700 \text{ cm}^{-1}$, which is characteristic of crystalline T- Nb_2O_5 (see Fig. 14). For $\text{Nb}_2\text{O}_5/\text{Al}_2\text{O}_3$, further calcination at 700 °C does not shift the Raman band at $\sim 650 \text{ cm}^{-1}$ [1]. Thus, it appears that on SiO_2 the surface niobium oxide phase at high loading is present as a bulk Nb_2O_5 phase which weakly interacts with the silica substrate, and that on Al_2O_3 the supported niobium oxide phase at high loading is present as a two-dimensional overlayer anchored to the alumina support. The complete absence of Raman bands at $\sim 650 \text{ cm}^{-1}$ for $\text{Nb}_2\text{O}_5/$

MgO at high loading reveals that the extremely basic MgO support dominates the surface pH. In addition, crystalline Nb₂O₅ could not be formed at extremely high Nb₂O₅ loading, ~15 wt.% Nb₂O₅/MgO, which corresponds to approximately two monolayers of surface niobium oxide for this MgO support of ~80 m² g⁻¹. The inability to form crystalline Nb₂O₅ at high loadings and the very basic nature of the Nb₂O₅/MgO surface, absence of ~650 cm⁻¹ Raman band at high loadings, is related to the strong acid–base interaction between Nb₂O₅ and MgO, and leads to significant incorporation of Nb⁺⁵ into the MgO support surface. This is also consistent with XPS surface measurements of the Nb₂O₅/MgO system, which show a linear increase of the [Nb/Mg]_{surface} ratio with increasing Nb₂O₅ loading to ~15 wt.%. The strong vibrations of the TiO₂ and ZrO₂ supports in the ~650 cm⁻¹ region prevented the direct detection of this species at high loadings of Nb₂O₅.

It is well known that surface metal oxides on oxide supports are stable to high calcination temperatures and prevent the dehydroxylation of the oxide supports [6, 7]. In this study, niobium oxide reacts with the surface hydroxyl groups of the oxide supports (MgO, Al₂O₃, TiO₂, ZrO₂ and SiO₂) to form a surface niobium oxide overlayer which retards the loss in surface areas of the Al₂O₃, TiO₂, ZrO₂ and SiO₂ supports at elevated calcination temperatures (see Table 1). However, the presence of niobium oxide does not stabilize the MgO surface area at 950 °C calcination temperature, due to the formation of a Nb–Mg–O solid solution.

The different molecular states of niobium oxide (crystalline Nb₂O₅, compounds, and surface niobium oxide phase) can be discriminated via Raman spectroscopy, since it monitors the structural transformations of the supported niobium oxide systems with increasing temperature. The surface niobium oxide overlayer on the oxide supports (Al₂O₃, TiO₂, ZrO₂ and SiO₂) is stable to high calcination temperatures (300–950 °C) because of the strong surface niobium oxide phase–oxide support interaction. The 5 wt.% Nb₂O₅/Al₂O₃ sample calcined between 500 and 950 °C exhibits only the Raman bands of the surface niobium oxide phase, and no evidence for the formation of crystalline Nb₂O₅ and AlNbO₄ phases is found (see Fig. 7) [1, 13]. During thermal treatments, an increase in surface density of the supported niobium oxide phase occurs on decreasing the surface area of the oxide support [28], which shifts the Raman band from ~900 to ~930 cm⁻¹ in the Nb₂O₅/ZrO₂ system (see Fig. 11). Raman studies also reveal that the surface niobium oxide overlayer on TiO₂ is partially transformed to crystalline H–Nb₂O₅ (characteristic Raman band at ~1000 cm⁻¹) due to the loss in surface area of TiO₂ treated at a temperature greater than 800 °C (see Fig. 9). Upon increasing the temperature of treatment from 800 to 950 °C, the decrease in Raman band intensity at ~1000 cm⁻¹ indicates that the crystalline H–Nb₂O₅ reacts with TiO₂ to form a Nb–Ti–O phase at high calcination temperature [29]. Bulk Nb₂O₅ is not stable to elevated calcination temperatures, and exhibits a phase transformation of amorphous Nb₂O₅ to H–Nb₂O₅ due to the weak interaction with the SiO₂ support (see Fig. 14). Thus, the surface

niobium oxide phase–oxide support interaction controls the thermal stability of the surface niobium oxide phases.

Recent EXAFS/XANES studies on Al_2O_3 , TiO_2 and SiO_2 -supported niobium oxide catalysts have been reported by Nishimura *et al.* [30, 31]. At low Nb_2O_5 loadings (<3 wt.%), they determined that the surface niobium oxide phases possess a dioxo NbO_4 structure on the Al_2O_3 as well as SiO_2 supports and a mono-oxo NbO_5 structure on the TiO_2 support. A model for a monolayer of surface niobium oxide on silica, $\sim 320 \text{ m}^2 \text{ g}^{-1}$, corresponding to ~ 23.7 wt.% $\text{Nb}_2\text{O}_5/\text{SiO}_2$ was presented, and it was concluded that the Nb–O and Nb–Nb bond lengths of the surface niobium oxide monolayer are similar to those of T- Nb_2O_5 [32]. The SiO_2 -supported niobium oxide catalysts were also studied by Weissman *et al.* [33], who determined that a monolayer of surface niobium oxide on silica, $\sim 300 \text{ m}^2 \text{ g}^{-1}$, corresponds to ~ 29.3 wt.% $\text{Nb}_2\text{O}_5/\text{SiO}_2$. The surface niobium oxide monolayer contains no crystalline Nb_2O_5 phase from X-ray diffraction [33].

The valence sum rule is a useful concept for discussing the feasibility of a proposed surface niobium oxide structure [34]. The sum of the valencies or bond orders of the individual Nb–O bonds should equal to 5 ± 0.1 valence units. An empirical expression relating Nb–O bond length to bond valency was developed by Brown and Wu [35]. The Nb valence units of Nishimura's proposed models for surface niobium oxide phases on the Al_2O_3 , TiO_2 and SiO_2 supports are estimated to be 4.3, 3.6 and 5.7, respectively. These values are much lower or higher than the Nb^{+5} valence state (5 ± 0.1 v.u.). In addition, the ratio of the Nb^{+5} ionic radius to the O^{-2} ionic radius, 0.5, is too large to fit into a NbO_4 tetrahedral structure. Thus, Nishimura's models for the surface niobium oxide phases are less feasible. No crystalline Nb_2O_5 phase was detected on the $\text{Nb}_2\text{O}_5/\text{SiO}_2$ systems at high Nb_2O_5 loadings from XRD. This suggests that the bulk Nb_2O_5 phase on the SiO_2 support possesses a particle size smaller than 40 Å.

Conclusions

Raman and XPS studies on supported niobium oxide catalysts under ambient conditions reveal that the surface niobium oxide phase forms a two-dimensional overlayer on oxide supports (MgO , Al_2O_3 , TiO_2 , ZrO_2 and SiO_2). The available Raman data under ambient conditions on supported niobium oxide catalysts, consistent with prior studies indicate that the surface pH determines the molecular structures of the surface metal oxide phases. At low surface coverages on basic oxide supports (MgO and Al_2O_3), hexaniobate-like surface species ($\text{H}_x\text{Nb}_6\text{O}_{19}^{-(8-x)}$ where $x = 1, 2, 3$) appear to be present. The hexaniobate-type surface species contain highly distorted NbO_6 octahedra. At high surface coverages on basic (Al_2O_3) and acidic (TiO_2 and ZrO_2) oxide supports, hydrated niobium oxide-type surface species ($\text{Nb}_2\text{O}_5 \cdot n\text{H}_2\text{O}$) are also present. The hydrated niobium oxide-type surface species contain slightly distorted NbO_6 octahedra as well as slightly distorted NbO_7 and NbO_8

structures. The hydrated niobium oxide-type surface species probably also predominate at low surface coverages on the acidic oxide supports (TiO_2 , ZrO_2 and SiO_2), but cannot be detected due to overlap with the strong vibrations from the oxide supports. In addition, bulk Nb_2O_5 Raman bands at $\sim 680 \text{ cm}^{-1}$ could be observed above 19 wt.% $\text{Nb}_2\text{O}_5/\text{Al}_2\text{O}_3$, 5 wt.% $\text{Nb}_2\text{O}_5/\text{ZrO}_2$ and 2 wt.% $\text{Nb}_2\text{O}_5/\text{SiO}_2$ indicating that monolayer coverage, titration of reactive surface hydroxyls, had been achieved. These conclusions are also supported by the XPS measurements. Bulk Nb_2O_5 was not formed on MgO , even at the equivalent of two monolayers loading, and could not be detected on TiO_2 because of the very strong TiO_2 vibrations. The XPS measurements of the surface niobium oxide on TiO_2 suggest that the monolayer coverage is reached at ~ 7 wt.% $\text{Nb}_2\text{O}_5/\text{TiO}_2$. The surface niobium oxide phase on oxide supports (such as Al_2O_3 , TiO_2 , ZrO_2 and SiO_2) is stable to high calcination temperatures. The high temperature stability of the surface niobium oxide overlayer is due to the strong interaction between the surface niobium oxide phase and these oxide supports.

Acknowledgement

Financial support for this work by Niobium Products Company, Inc. is gratefully acknowledged. We wish to thank P. McCaslin of Unocal Science and Technology Division for the XPS measurements.

References

- 1 J. M. Jehng and I. E. Wachs, *Prepr. Am. Chem. Soc., Div. Petrol. Chem.*, 34 (1989) 546.
- 2 E. I. Ko, R. Bafrafi, N. T. Nuhfer and N. J. Wagner, *J. Catal.*, 95 (1985) 260.
- 3 Y. Wada, M. Inaida, Y. Murakami and A. Morikawa, *Bull. Chem. Soc. Jpn.*, 61 (1988) 3839.
- 4 A. M. Turek, I. E. Wachs and E. Delanio, to be published.
- 5 I. E. Wachs, *Proc. Int. Conf. Niobium and Tantalum, Orlando, Nov. 7-9, 1988*, Tantalum-Niobium Int. Study Center, Brussels, 1989, p. 679.
- 6 *U.S. Pat. 4 415 480* (1983) to L. L. Murrell and D. C. Grenoble.
- 7 I. E. Wachs, J. M. Jehng and F. D. Hardcastle, *Solid State Ionics*, 32/33 (1989) 904.
- 8 L. L. Murrell, D. C. Grenoble, C. J. Kim and N. C. Dispenziere, *J. Catal.*, 107 (1987) 463.
- 9 *U.S. Pat. 4 233 139* (1980) to L. L. Murrell, D. C. Grenoble and C. J. Kim.
- 10 S. Okazaki and T. Okuyama, *Bull. Chem. Soc. Jpn.*, 56 (1983) 2159.
- 11 K. Asakura and Y. Iwasawa, *Chem. Lett.*, (1986) 511.
- 12 K. Asakura and Y. Iwasawa, *Chem. Lett.*, (1988) 633.
- 13 J. M. Jehng and I. E. Wachs, *Chem. Mater.*, 3 (1991) 100.
- 14 J. M. Jehng and I. E. Wachs, *J. Raman Spectrosc.*, 22 (1991) 83.
- 15 S. S. Chan, I. E. Wachs, L. L. Murrell, L. Wang and W. K. Hall, *J. Phys. Chem.*, 88 (1984) 5831.
- 16 G. Deo and I. E. Wachs, *J. Phys. Chem.*, in press.
- 17 F. P. J. M. Kerkhof and J. A. Moulijn, *J. Phys. Chem.*, 83 (1979) 1612.
- 18 Z. X. Liu, Z. D. Lin, H. Fan and F. H. Li, *Appl. Phys.*, A45 (1988) 160.
- 19 I. E. Wachs, F. D. Hardcastle and S. S. Chan, *Spectroscopy*, 1 (1986) 30.
- 20 S. S. Chan, I. E. Wachs, L. L. Murrell and C. C. Dispenziere, Jr., *J. Catal.*, 92 (1985) 1.
- 21 W. S. Millman, K. I. Segawa, D. Smrz and W. K. Hall, *Polyhedron*, 5 (1986) 169.

- 22 C. L. O'Young, C. H. Yang, S. J. DeCanio, M. S. Patel and D. A. Storm, *J. Catal.*, **113** (1988) 307.
- 23 G. A. Park, *Chem. Rev.*, **65** (1965) 177; *idem*, *Adv. Chem. Ser.*, **61** (1967) 121.
- 24 Y. S. Yin, A. Ougour, A. Auroux and J. C. Vederine, *Stud. Surf. Sci. Catal.*, **48** (1989) 525.
- 25 F. J. Gil-Llambas, A. M. Escudey, J. C. G. Fierro and A. C. Agudo, *J. Catal.*, **95** (1985) 520.
- 26 A. Goiffon and B. Spinner, *Bull. Soc. Chim. Fr.* **11-12** (1975) 2435.
- 27 A. Goiffon, R. Granger, C. Bockel and B. Spinner, *Rev. Chim. Min.*, **10** (1973) 487.
- 28 F. Roozeboom, J. Medema and P. J. Gellings, *Z. Phys. Chem.*, **111** (1978) 215.
- 29 A. F. Well, *Structural Inorganic Chemistry*, Oxford, London, 1984.
- 30 M. Nishimura, K. Asakura and Y. Iwasawa, *J. Chem. Soc., Chem. Commun.*, (1986) 1660.
- 31 M. Nishimura, K. Asakura and Y. Iwasawa, in M. J. Phillips and M. Ternan (eds.), *Proc. 9th Int. Congr. Catal.*, Vol. 4, The Chemical Institute of Canada, Ottawa, 1988, p. 1842.
- 32 M. Shirai, A. Asakura and Y. Iwasawa, *PACIFICHEM '89, Catalytic Conversion with Niobium Materials*, Honolulu, Dec. 17-22, 1989; M. Shirai, N. Ichikuni, K. Asakura and Y. Iwasawa, *Catal. Today*, **8** (1990) 57.
- 33 J. G. Weissman, E. I. Ko and P. Wynblatt, *J. Catal.*, **108** (1987) 383.
- 34 I. D. Brown, *Chem. Soc. Rev.*, **7** (1978) 359.
- 35 I. D. Brown and K. K. Wu, *Acta Cryst.*, **B32** (1976) 1957.